Glaucoma

Retinal Nerve Fiber Layer Damage Assessment in Glaucomatous Eyes Using Retinal Retardance Measured by Polarization-Sensitive Optical Coherence Tomography

Reshma Radhakrishnan Parakkel[1], Damon Wong[1–3], Chi Li[1,2], Jocelyn Cheong[1,3], Monisha Esther Nongpiur[1,3], Rachel Shujuan Chong[1,3], Tin Aung[1,3,4], Leopold Schmetterer[1–8], Xinyu Liu[1–3], and Jacqueline Chua[1–3]

[1] Singapore Eye Research Institute, Singapore National Eye Centre, Singapore, Singapore
[2] SERI-NTU Advanced Ocular Engineering (STANCE) Program, Singapore, Singapore
[3] Ophthalmology & Visual Sciences Academic Clinical Programme, Duke-NUS Medical School, Singapore, Singapore
[4] Department of Ophthalmology, Yong Loo Lin School of Medicine, National University of Singapore, Singapore, Singapore
[5] School of Chemistry, Chemical Engineering and Biotechnology, Nanyang Technological University, Singapore, Singapore
[6] Department of Clinical Pharmacology, Medical University of Vienna, Vienna, Austria
[7] Center for Medical Physics and Biomedical Engineering, Medical University of Vienna, Vienna, Austria
[8] Institute of Molecular and Clinical Ophthalmology, Basel, Switzerland

Correspondence: Xinyu Liu, Singapore Eye Research Institute, Singapore National Eye Centre, 20 College Road, Singapore 169856, Singapore. e-mail: liu.xinyu@seri.com.sg
Jacqueline Chua, Singapore Eye Research Institute, Singapore National Eye Centre, 20 College Road, Singapore 169856, Singapore. e-mail: jacqueline.chua.y.m@seri.com.sg

Purpose: To assess the diagnostic performance and structure–function association of retinal retardance (RR), a customized metric measured by a prototype polarization-sensitive optical coherence tomography (PS-OCT), across various stages of glaucoma.

Methods: This cross-sectional pilot study analyzed 170 eyes from 49 healthy individuals and 68 patients with glaucoma. The patients underwent PS-OCT imaging and conventional spectral-domain optical coherence tomography (SD-OCT), as well as visual field (VF) tests. Parameters including RR and retinal nerve fiber layer thickness (RNFLT) were extracted from identical circumpapillary regions of the fundus. Glaucomatous eyes were categorized into early, moderate, or severe stages based on VF mean deviation (MD). The diagnostic performance of RR and RNFLT in discriminating glaucoma from controls was assessed using receiver operating characteristic (ROC) curves. Correlations among VF-MD, RR, and RNFLT were evaluated and compared within different groups of disease severity.

Results: The diagnostic performance of both RR and RNFLT was comparable for glaucoma detection (RR AUC = 0.98, RNFLT AUC = 0.97; $P = 0.553$). RR showed better structure–function association with VF-MD than RNFLT (RR VF-MD = 0.68, RNFLT VF-MD = 0.58; $z = 1.99$; $P = 0.047$) in glaucoma cases, especially in severe glaucoma, where the correlation between VF-MD and RR ($r = 0.73$) was significantly stronger than with RNFLT ($r = 0.43$, $z = 1.96$, $P = 0.050$). In eyes with early and moderate glaucoma, the structure–function association was similar when using RNFLT and RR.

Conclusions: RR and RNFLT have similar performance in glaucoma diagnosis. However, in patients with glaucoma especially severe glaucoma, RR showed a stronger correlation with VF test results. Further research is needed to validate RR as an indicator for severe glaucoma evaluation and to explore the benefits of using PS-OCT in clinical practice.

Translational Relevance: We demonstrated that PS-OCT has the potential to evaluate the status of RNFL structural damage in eyes with severe glaucoma, which is currently challenging in clinics.

translational vision science & technology

Introduction

Regular eye examinations to monitor the disease progression are an essential part of clinical glaucoma management. Currently, spectral-domain optical coherence tomography (SD-OCT) imaging[1,2] and visual field (VF) testing[3,4] are standard approaches to aid glaucoma diagnosis and monitoring structural and functional damage. SD-OCT provides a three-dimensional scan of the retina and measures the thickness of retinal nerve fiber layer (RNFL), thereby enabling a quantitative evaluation of the degeneration of retinal ganglion cells.[1,2] An SD-OCT scan takes 5 to 10 seconds and is relatively easy to perform; however, the measurement is prone to segmentation errors due to the inaccuracy in delineating the boundaries of the RNFL.[5–7] Moreover, as the glaucoma progresses to advanced stages, the segmentation of the RNFL layer from retinal intensity B-scans becomes difficult due to the confounding presence of glial and vascular tissues, which may compromise the reliability of SD-OCT evaluation in patients with severe glaucoma.[5,8,9] VF testing is effective in monitoring the progress of severe glaucoma by measuring regional vision loss across the entire VF.[10] However, VF tests require longer testing time (several minutes), and the results are less reliable in patients who are not able to cooperate well,[3] leading to variability in the test results.[11] Therefore, additional diagnostic approaches to clinically evaluate the development and progression of glaucoma are needed.

Polarization-sensitive optical coherence tomography (PS-OCT) imaging extends the contrast of conventional OCT imaging with the measurement of tissue birefringence.[12–14] Birefringence arises in biological tissues where the microstructure is anisotropically organized (e.g., aligned fibers).[13,15] PS-OCT measurements including retardance and depth-resolved birefringence of the RNFL in healthy human eyes have been documented.[12,15–18] In glaucomatous eyes, the birefringence of RNFL is expected to be lower than that in heathy eyes[15] due to a disordered RNFL structure and loss of nerve fibers. Reduction in RNFL birefringence in glaucomatous eyes has been observed in a few cases[14,15] and recently validated in a clinical study.[15] However, most of these studies assumed that the loss or change in birefringence occurs before the loss of RNFL thickness (RNFLT) and accordingly focused on the potential of PS-OCT as an approach to detect early glaucoma.[14,15,17,19,20] There is a gap in our understanding regarding the diagnostic performance of RNFL birefringence in eyes with moderate and severe glaucoma. Furthermore, the advantages and disadvantages of utilizing PS-OCT as an indicator for assessing glaucoma severity in comparison to existing approaches remain unclear.

In this pilot study, we aimed to assess the potential of using retinal retardance (RR), a metric derived from the cumulative birefringence from the surface of the retina to the retinal pigment epithelium (RPE), to assess the structural damage in glaucomatous eyes across various stages of severity. RR is measured by triple-input PS-OCT,[21] a novel modulation configuration of PS-OCT recently developed by our group, which has an improved sensitivity compared to sequential dual-input PS-OCT. In contrast to measuring RNFLT in SD-OCT, PS-OCT measurements of retinal retardance are not influenced by blood vessels, given their low-birefringent nature. Additionally, the RR measurement do not require segmentation of the boundaries of the RNFL, as the low-birefringent layers of the retina do not contribute to the RR measurement. Based on this, our hypothesis is that RR would be a more reliable indicator than RNFLT in eyes with advanced glaucoma. The measurement of RR would be less prone to measurement errors resulting from inaccurate RNFL segmentation in advanced glaucomatous eyes, as observed in conventional SD-OCT.

Methods

Participants

This pilot study adhered to the tenets of the Declaration of Helsinki and was approved by the SingHealth Centralized Institutional Review Board (reference no. R1687/10/2020). Prior to enrolment, all participants gave their written informed consent. From April 21, 2021, to June 15, 2023, we recruited 117 participants from the Singapore National Eye Center, including 49 healthy individuals and 68 patients diagnosed with glaucoma (summarized in Fig. 1A). All recruited subjects underwent PS-OCT and SD-OCT scans for both eyes, but only patients diagnosed with bilateral glaucoma underwent VF tests.

The diagnosis of glaucoma was established through a clinical examination that assessed the presence of glaucomatous optic neuropathy with glaucomatous VF loss. We classified the severity of glaucoma based on the mean deviation (MD) of the VF as early stage (MD ≥ -6 dB), moderate stage (-6 dB $>$ MD ≥ -12dB), or severe stage (MD < -12 dB),[22] with reliability thresholds for fixation losses set at $\leq 20\%$ and false positives and false negatives set at $\leq 15\%$.

Our control group consisted of individuals without glaucoma or any clinically relevant eye conditions
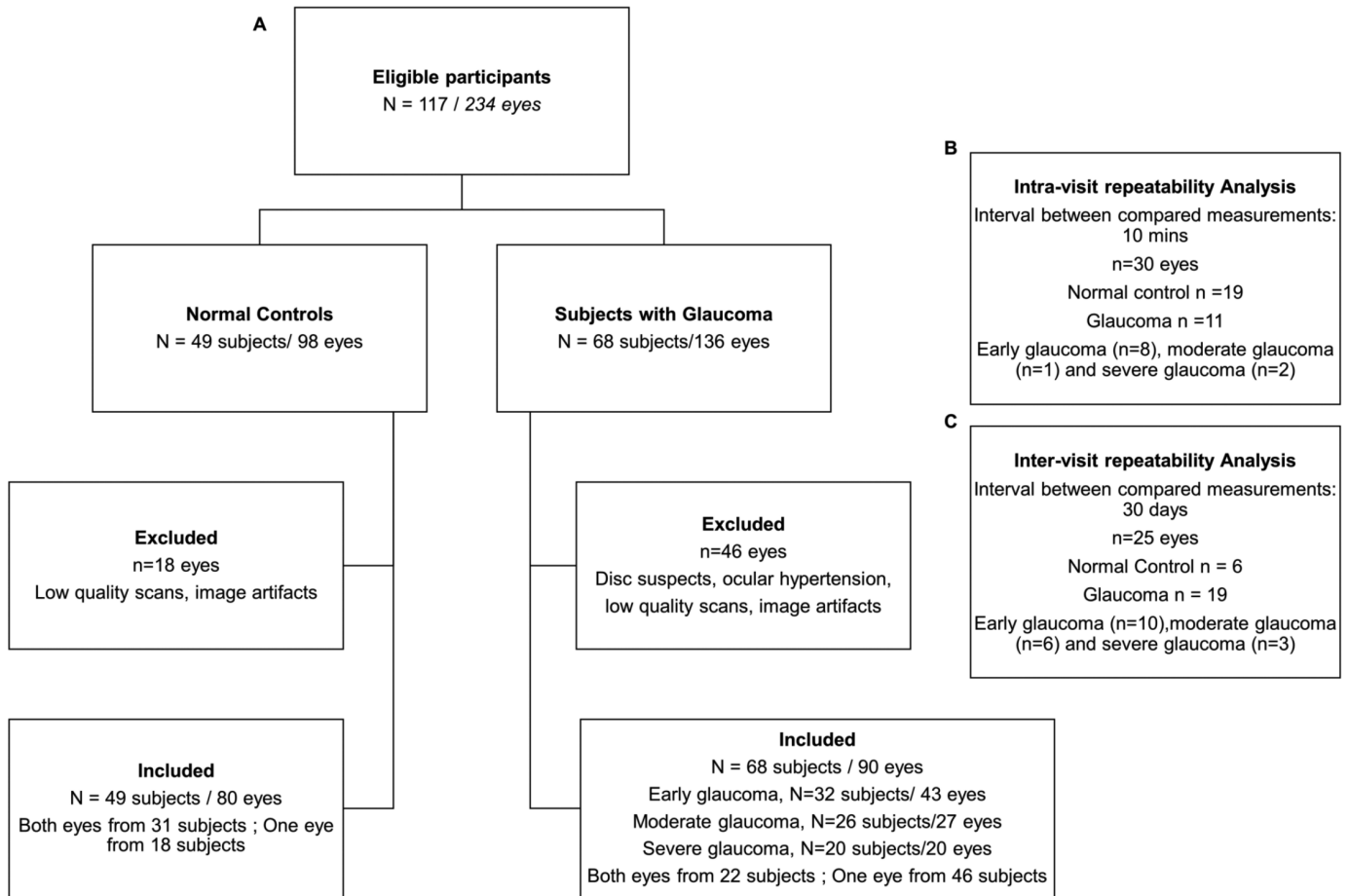
Figure 1. (**A**) Diagram summarizing patient recruitment in the pilot study. (**B**) Intravisit repeatability study. (**C**) Intervisit repeatability study. The grouping of glaucoma severity was based on eyes; that is, the two eyes of some subjects were grouped into different groups.

that could affect retinal thickness, such as macular or vitreoretinal diseases, diabetic retinopathy, age-related macular degeneration, or other retinopathies. We excluded participants who showed signs of retinal or optic neuropathies other than glaucoma, had a history of retinal surgery or laser treatments, had visual acuity worse than 6/15, or had systemic diseases that could influence the retina or visual field. Eyes with non-glaucomatous optic neuropathies and conditions such as ocular hypertension were removed from the analysis (14 eyes). Participants self-reported their sex and ethnicity.

SD-OCT Imaging

SD-OCT imaging was performed using a commercially available CIRRUS HD-OCT 6000 system (Carl Zeiss Meditec, Dublin, CA) based on the inbuilt $6 \times 6\text{-mm}^2$ scan protocol centered on the optic nerve head. This protocol generates a cube of data through a 6-mm square grid, acquiring a series of 200 horizontal scan lines each composed of 200 A-scans.[23] The inbuilt software was used to generate the RNFLT map by measuring the thickness of the RNFL from the retinal structural images. Simultaneously, a thickness deviation map was generated to display abnormal RNFLT less than the lower 95th or 99th percentile of the normal range at the $6 \times 6\text{-mm}^2$ parapapillary area. Each scan was manually reviewed with Zeiss CIRRUS HD-OCT Review Software 11.5.1, and six eyes out of 234 eyes (3%) were excluded due to poor-quality scans characterized by the presence of segmentation artifacts, inconsistent signal intensity across a scan, extremely low signal, or substantial motion artifacts.

PS-OCT Imaging

The PS-OCT used in this pilot study was recently developed by our group, and we refer to it as triple-input PS-OCT,[21] and it has demonstrated an improved

detection sensitivity compared to sequential dual-input PS-OCT. Briefly, to measure the birefringence of the retina, a novel triple-state modulator was used to modulate the probing light into three polarization states that were mutually orthogonal on the Poincaré sphere. The triple-input PS-OCT prototype utilized a swept-source laser (Axsun Technologies, Billerica, MA) that produces light sweeping at 200 kHz with a central wavelength of 1060 nm and a sweeping range of 100 nm, providing a theoretical axial resolution of 6 μm. The scanning beam diameter at the pupil was 0.67 mm, providing an optical lateral resolution of 44 μm and a depth of focus of 2.9 mm in a typical human eye. The spatial averaging in the birefringence reconstruction, including filtering of Stokes vectors and spectral binning,[13] reduced the resolution to 150 μm in the lateral and 30 μm in the axial directions for birefringence imaging. A raster scan of the laser spot on the retina was performed covering an 8 × 8-mm square area centered on the optic nerve head (ONH) and consisting of 700 × 700 A-lines.

To evaluate the repeatability of the PS-OCT retardance measurement during a single visit, an analysis was performed involving a subcohort of 21 volunteers; nine subjects contributed both eyes and 12 subjects each contributed one eye to the study. This group was comprised of 13 individuals without glaucoma who served as normal controls and eight subjects diagnosed with glaucoma. Specifically, all participants underwent an additional PS-OCT scan conducted 10 minutes after the initial scan (Fig. 1B).

Moreover, a study was carried out to assess the consistency of PS-OCT measurements across different visits and to investigate the intervisit repeatability of PS-OCT measurements. This investigation involved 25 eyes from 14 individuals, including six eyes without glaucoma and 19 eyes from subjects with glaucoma (10 eyes with early-stage glaucoma, six eyes with moderate glaucoma, and three eyes with severe glaucoma). All participants were requested to return for a follow-up visit 30 days after their initial visit for a second PS-OCT scan (Fig. 1C).

Before proceeding to data analysis, we manually checked the PS-OCT scans by previewing the intensity B-scans using ImageJ (National Institutes of Health, Bethesda, MD); 39 out of 234 eyes (17%), apart from the six eyes excluded during the SD-OCT preview, were excluded due to quality issues characterized by low image intensity, out-of-range scans, or strong motion artifacts.

Analysis of Retinal Retardance and RNFLT Maps

For PS-OCT, the retinal retardance was measured from cumulative birefringence of the retina extending from the retinal surface to the RPE layer. Specifically, a scan volume consisting of 700 × 700 A-lines was generated by stacking retinal B-scans sequentially. The en face intensity map was synthesized by an average projection of the volume data along depth, creating an image that is similar to a fundus photograph (Fig. 2A). A customized MATLAB (MathWorks, Natick, MA) algorithm was developed to detect the surface of the retina and the RPE layer in each B-scan. The retinal region was segmented from each B-scan by selecting the area between the surface of the retina and the RPE layer. Manual review and corrections were performed when necessary to ensure a precise segmentation. A vectorial birefringence map[24] was derived and followed by a summation of the birefringence vectors within the segmented retinal region along the depth to obtain the RR en face map (Fig. 2B). Note that, in contrast to conventional SD-OCT image analysis, the PS-OCT RR
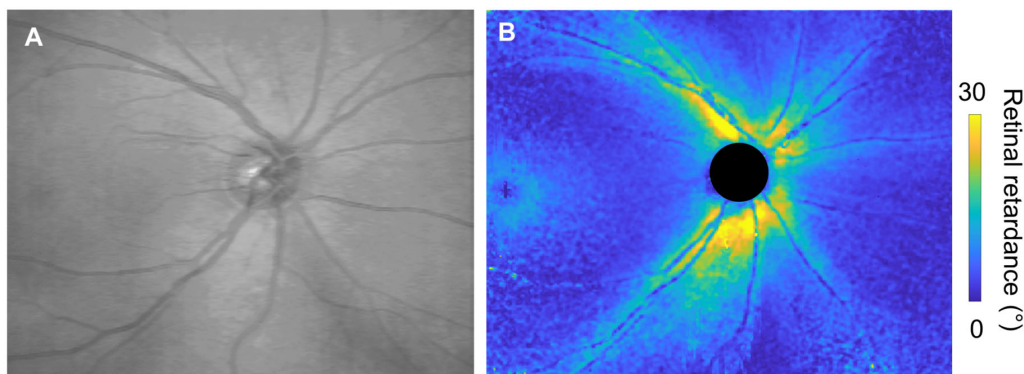

Figure 2. Representative PS-OCT scans of a healthy eye. (**A**) En face intensity map. (**B**) En face retinal retardance maps projected from the retina, which is defined as the tissue between the retinal surface and RPE layer in the PS-OCT scan.

measurement does not require the segmentation of the lower boundary of the RNFL.

The extraction of RNFL parameters from RR en face retardance maps was similar to the algorithm utilized by the CIRRUS HD-OCT 6000 for analyzing RNFLT. Specifically, we computed the global RR and global RNFLT values from the en face maps obtained from the same annular circumpapillary region under both PS-OCT and SD-OCT. This annular region had an inner diameter of 1.2 mm and an outer diameter of 3.46 mm, centered on the ONH. Additionally, we divided the circumpapillary region into four quadrants around the ONH—namely, superior, nasal, inferior, and temporal. For each quadrant, we calculated the average retardance and thickness values.

Visual Field

The VF central 24-2 threshold test was performed using the Zeiss Humphrey Field Analyzer 3 with the Swedish Interactive Threshold Algorithm (SITA) Fast algorithm.[25] The average testing time for each eye was around 3 to 5 minutes, after which the visual field mean deviation (VF-MD) was extracted from the generated single field analysis report.[26]

Statistical Analysis

Age and axial length were compared between normal controls and the glaucoma groups using the Mann–Whitney U test, and sex was compared using the χ^2 test. The diagnostic metrics were adjusted for age, axial length, gender, and inter-eye correlation using a generalized estimating equation when calculating the association between the metrics and severity of glaucoma.[27,28] The repeatability of retardance measurements was analyzed using Bland–Altman plots, and correlations between the first and second measurements were further assessed by the intraclass correlation coefficient (ICC). Correlation analyses, including repeatability among retardance measurements, RR versus RNFLT, VF-MD versus RR, and RNFLT were conducted using Spearman's correlation. Receiver operating characteristic (ROC) curves were used to evaluate the performance of RNFLT and

RR values as the diagnostic parameters for glaucoma detection. Performance calculations of both metrics were also adjusted for age, axial length, and gender by simultaneously including the confounder variables as predictors in a logistic regression model.[27] The evaluation metrics for glaucoma detection were the area under the ROC curve (AUC), sensitivity, and specificity. To adjust for intra-eye correlations, 95% confidence intervals (CIs) were generated after bootstrapping. Differences in AUCs between diagnostic parameters were compared by two-sided Delong tests.[29] The correlation analyses of VF-MD with RR and RNFLT were statistically compared by Fisher's r-to-z transformation.[30] All statistical analyses were performed using MATLAB.

Results

After quality assessment and data selection, the analysis involved a total of 170 eyes, including 80 eyes from 49 normal controls and 90 eyes from 68 patients with primary open-angle glaucoma (43 early glaucoma eyes, 27 moderate glaucoma eyes, and 20 severe glaucoma eyes). We found that there was a statistically significant difference in age and gender between the normal control and glaucoma groups (Table 1). The normal control group had a younger mean age of 43 ± 16 years, whereas the glaucoma patients had an older mean age of 67 ± 9 years ($P < 0.001$). Additionally, the normal control group had a lower percentage of male subjects (37%) compared to the glaucoma group (63%). Furthermore, there was a statistically significant difference in the axial length of the eyes in both groups, as eyes in the normal control group (axial length = 25.12 mm) were slightly longer than the glaucomatous eyes (24.47 mm) in the analysis ($P < 0.05$). In the subsequent analysis, we accounted for the potential influence of age, axial length, and gender by adjusting for these variables.

During the repeatability test conducted on 30 eyes, the PS-OCT demonstrated excellent repeatability in global circumpapillary regions, as well as the quadrants, with a strong Spearman's correlation coefficient of $r = 0.94$ ($r = 0.80$ for normal controls

Table 1. Characteristics of Subjects and Eyes Included in the Pilot Study

	Normal Controls ($n = 49$)	Glaucoma Participants ($n = 68$)	P
Age (yr), mean (SD)	42.12 (15.67)	66.04 (8.46)	**<0.001**
Male gender, n (%)	18 (37)	43 (63)	**<0.001**

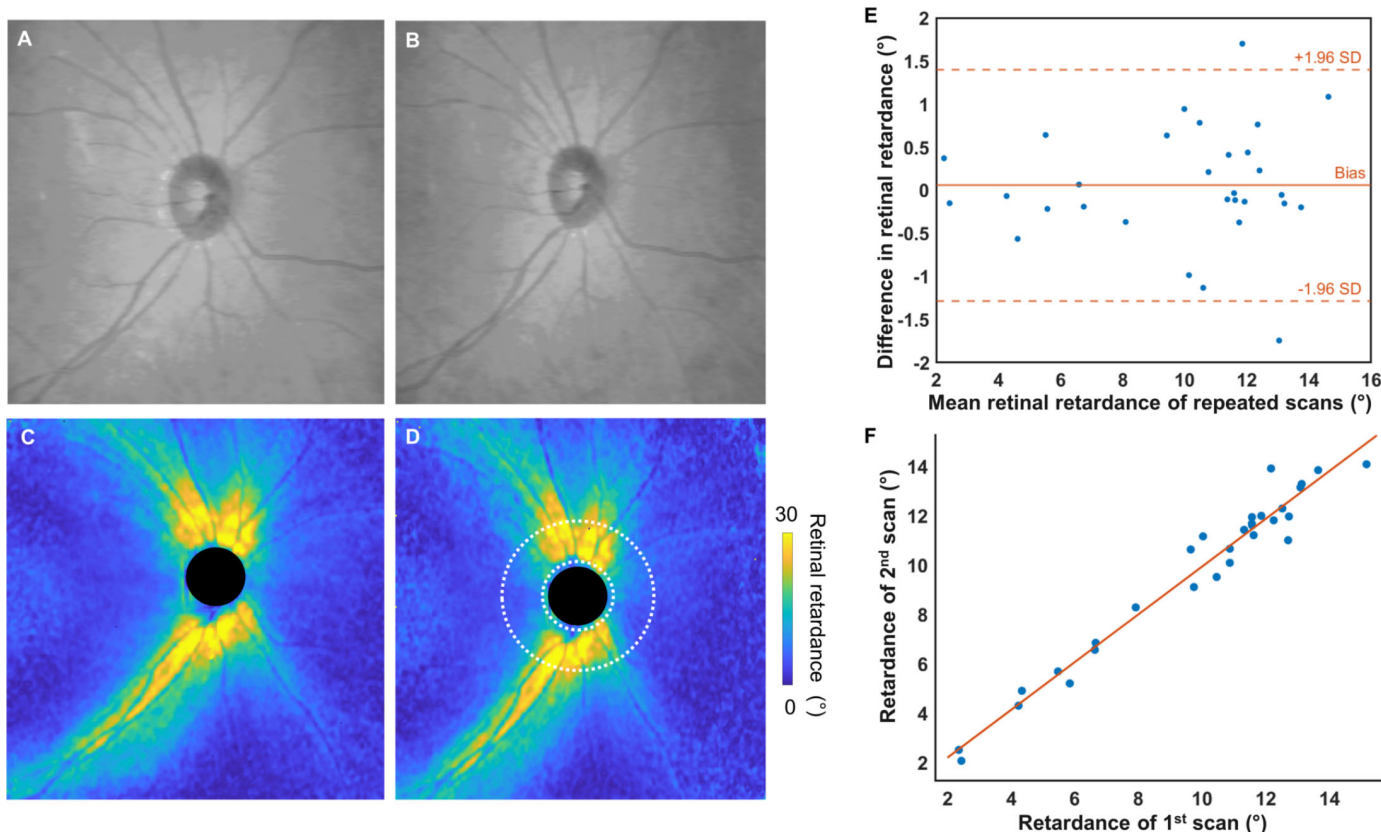Boldface values indicate statistical significance at $P < 0.05$.

Figure 3. Intravisit repeatability test of the PS-OCT system. (**A**, **B**) En face intensity maps of two PS-OCT scans of the right eye of a healthy subject with a 10-minute interval. (**C**, **D**) Corresponding en face retardance maps. The retinal retardance value is calculated as the average value of a circumpapillary annular region enclosed by *white dotted lines* in (**D**). The circumpapillary annular was defined by an inner radius of 0.6 mm and an outer radius of 1.73 mm. (**E**) Bland–Altman plot of the repetitive retinal retardance measurements. (**F**) Scatterplot of the repetitive retinal retardance measurements ($n = 30$ eyes, $r = 0.94$, $P < 0.001$; normal controls: $n = 19$ eyes, $r = 0.80$, $P < 0.001$; glaucoma subjects: $n = 11$ eyes, $r = 0.97$, $P < 0.001$). ICC = 0.98 (95% CI, 0.96–0.99).

and $r = 0.97$ for glaucoma subjects). The repeatability in the RR measurements was further confirmed by repetitive measurements falling within a narrow range of 0.1° (with a SD of 0.68°, within 0.6% of the mean retardance value) as shown in the Bland–Altman plot (Fig. 3, Table 2), and a high ICC = 0.98.

To ensure the reliability of PS-OCT measurements across different visits of a subject, we performed an intervisit repeatability assessment involving 25 eyes comparing measurements from two clinical visits acquired within an interval of 30 days. The retardance measurements displayed high repeatability with a Spearman's correlation coefficient of $r = 0.92$ and a high ICC = 0.94 (Fig. 4, Table 2).

As expected, we found that both RR and RNFLT were significantly lower for the glaucoma group than the normal control group (global RR: normal = 10.92 $\pm$ 1.85° and glaucoma = 5.93 $\pm$ 1.51°, $P < 0.001$; global RNFLT: normal = 96.68 $\pm$ 10.74 μm and glaucoma = 67.4 $\pm$ 10.50 μm, $P < 0.001$) (Table 3). Further-

more, we observed a strong correlation between the two parameters across all of the eyes ($r = 0.94$, $P < 0.001$) (Fig. 5).

We also compared the diagnostic performance of RR and RNFLT in terms of AUC as a classifier with and without adjusting for age, gender, and axial length. Overall, both metrics had similar diagnostic performance in univariate models (RR AUC = 0.98; RNFLT AUC = 0.97; $P = 0.553$) and multivariate models (RR AUC = 0.99; RNFLT AUC = 0.99; $P = 0.737$) (Table 4).

Upon inspection of the RR map from PS-OCT, RNFLT measurements and thickness deviation maps from SD-OCT, and the VF-MD (Fig. 6), we found that in eyes with severe glaucoma blood vessel patterns were discernible in the RNFLT map but were notably absent in the retinal retardance map (Figs. 6C, 6F). Furthermore, we extracted virtual circular B-scans (beginning at the superotemporal quadrant, as shown in Fig. 6C) centered at the ONH with a diameter of 3.5 mm

Table 2. Repeatability Assessment for Intrasubject Retardance Measurements

	Spearman's Correlation Coefficient (r)	P	ICC (95% CI)
Intravisit repeatability analysis performed on the same day, 10 minutes apart ($n = 30$ eyes); $n = 19$ for normal control and $n = 11$ for glaucoma (early glaucoma, $n = 8$; moderate glaucoma, $n = 1$; severe glaucoma, $n = 2$)			
Global	0.94	<0.001	0.98 (0.96–0.99)
Superior quadrant	0.97	<0.001	0.99 (0.98–0.99)
Nasal quadrant	0.94	<0.001	0.92 (0.84–0.96)
Inferior quadrant	0.96	<0.001	0.99 (0.98–1.00)
Temporal quadrant	0.91	<0.001	0.92 (0.83–0.96)
Intervisit repeatability analysis performed 1 month apart ($n = 25$ eyes); $n = 6$ for normal controls and $n = 19$ for glaucoma (early glaucoma, $n = 10$; moderate glaucoma, $n = 6$; severe glaucoma, $n = 3$)			
Global	0.92	<0.001	0.94 (0.87–0.97)
Superior quadrant	0.91	<0.001	0.92 (0.82–0.96)
Nasal quadrant	0.74	<0.001	0.87 (0.72–0.94)
Inferior quadrant	0.90	<0.001	0.88 (0.75–0.95)
Temporal quadrant	0.75	<0.001	0.79 (0.58–0.90)

(Fig. 7) of an eye with severe glaucoma and a normal control eye. Apart from the noticeable RNFL thinning, the scans indicated that retinal blood vessels extended beyond the upper RNFL surface in the glaucomatous eye, making precise RNFL layer segmentation difficult and consequently affecting the reliability of RNFLT measurement. However, from the distribution of retardance in the scan, it is evident that the retinal blood vessels show low retardance, as they are low birefringent in nature and are less likely to affect the RR measurement.

To assess the structure–function association in various glaucoma groups, we analyzed the correlation between VF-MD and RR or RNFLT in univariate models and multivariate models adjusted for age, gender, and axial length (Table 5). Pooling together eyes in all groups of disease stages, we found that both RR and RNFLT exhibited significant correlations with VF-MD (Figs. 8A, 8B), with RR exhibiting a stronger correlation with VF-MD than RNFLT ($z = 1.99$, $P = 0.047$). In contrast, in the group of early glaucoma, RNFLT and RR both showed low correlation coefficients (not statistically significant) with VF-MD in both univariate (Figs. 8C1, 8D1) and multivariate models. Within the groups of moderate and severe glaucoma, the correlation between RNFLT and RR is less significant than that in the early glaucoma group. However, both RR and RNFLT exhibited significant correlations with VF-MD (Figs. 8C2, 8C3, 8D2, 8D3). In eyes with severe glaucoma, RR exhibited a statistically significant higher correlation with VF-MD than RNFLT ($z = 1.96$, $P = 0.0496$), which suggests that RR could be a more reliable indica-

tor for the status of RNFL damage in advanced glaucoma.

Discussion

In this pilot study, we assessed the diagnostic performance of the RR measured by PS-OCT and compared the results with the standard RNFLT. We found that PS-OCT can provide reliable and repeatable measurements of RR in both normal and glaucoma subjects. Furthermore, we observed that both RR and RNFLT exhibit similar diagnostic performance for detecting glaucoma. We also discovered that RR in severe glaucoma demonstrated a stronger correlation with VF-MD than RNFLT, indicating that it may be less affected by RNFL segmentation errors. Specifically, the RNFLT thickness might be prone to inaccurate measurement over vessel regions[31] when the RNFL is thin in severe glaucoma.[5,8,9] Although a longitudinal study involving subjects with severe glaucoma would be necessary to further validate our observations, the results here show the potential of PS-OCT to provide a more accurate evaluation of disease progression in patients with severe glaucoma.

Previous PS-OCT–based studies have reported reductions in RNFL birefringence of eyes with glaucoma in a single case,[17,19] multiple cases,[14,20] and a cohort of subjects.[15] To the best of our knowledge, our report is the first cohort study to include patients with all stages of glaucoma and that analyzed the diagnostic performance of RR within groups of different
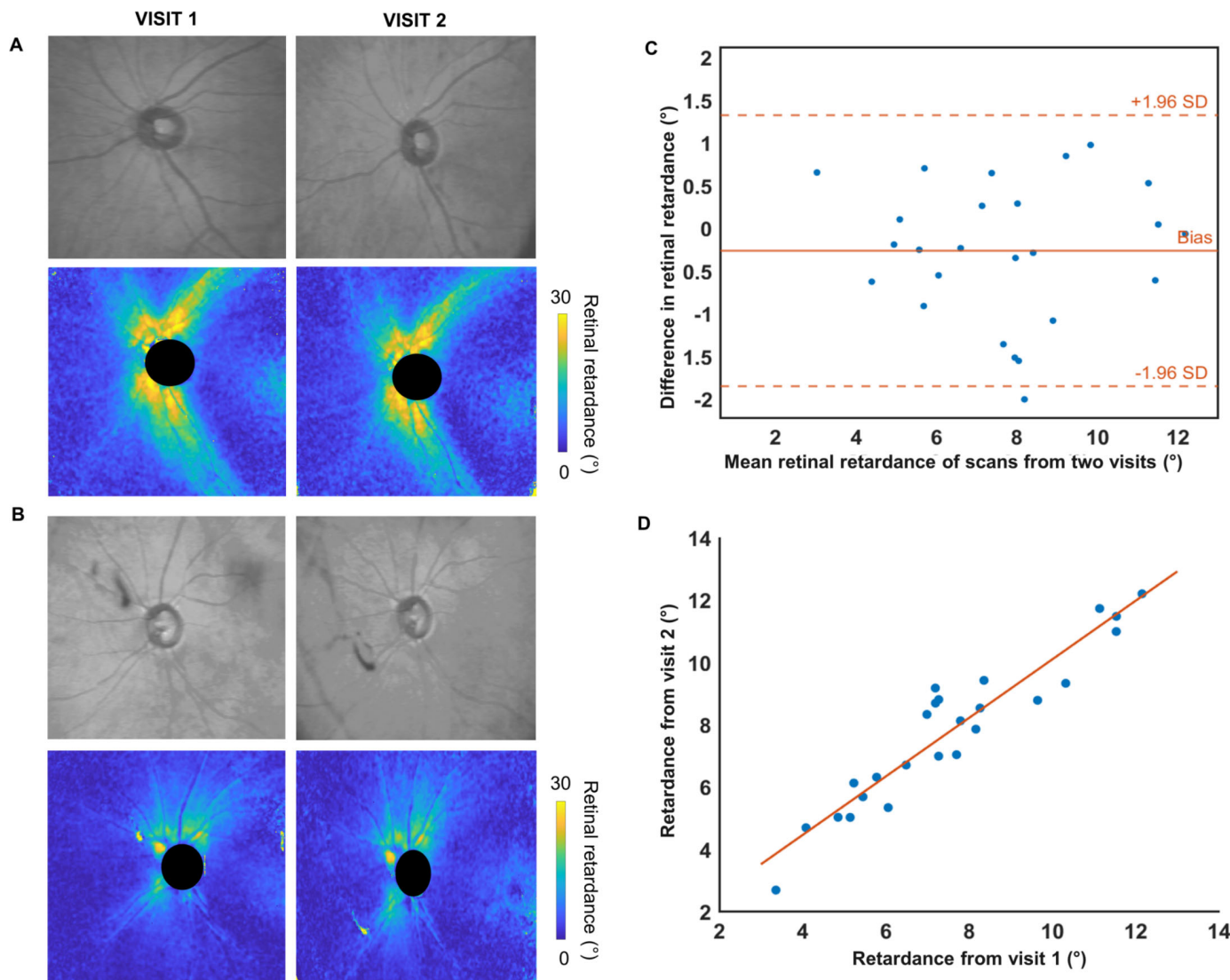
Figure 4. Intervisit repeatability test of the PS-OCT system. (**A**, **B**) En face intensity and retardance maps of two PS-OCT scans of a healthy eye (**A**) and an eye with early glaucoma (**B**) taken across two visits 30 days apart. (**C**) Bland–Altman plot of the repetitive retinal retardance measurements. (**D**) Scatterplot of the repetitive retinal retardance measurements ($n = 25$ eyes, $r = 0.92$, $P < 0.001$). ICC = 0.94 (95% CI, 0.87–0.97).

Table 3. Comparison of Diagnostic Parameters Between Normal Controls and Participants With Glaucoma

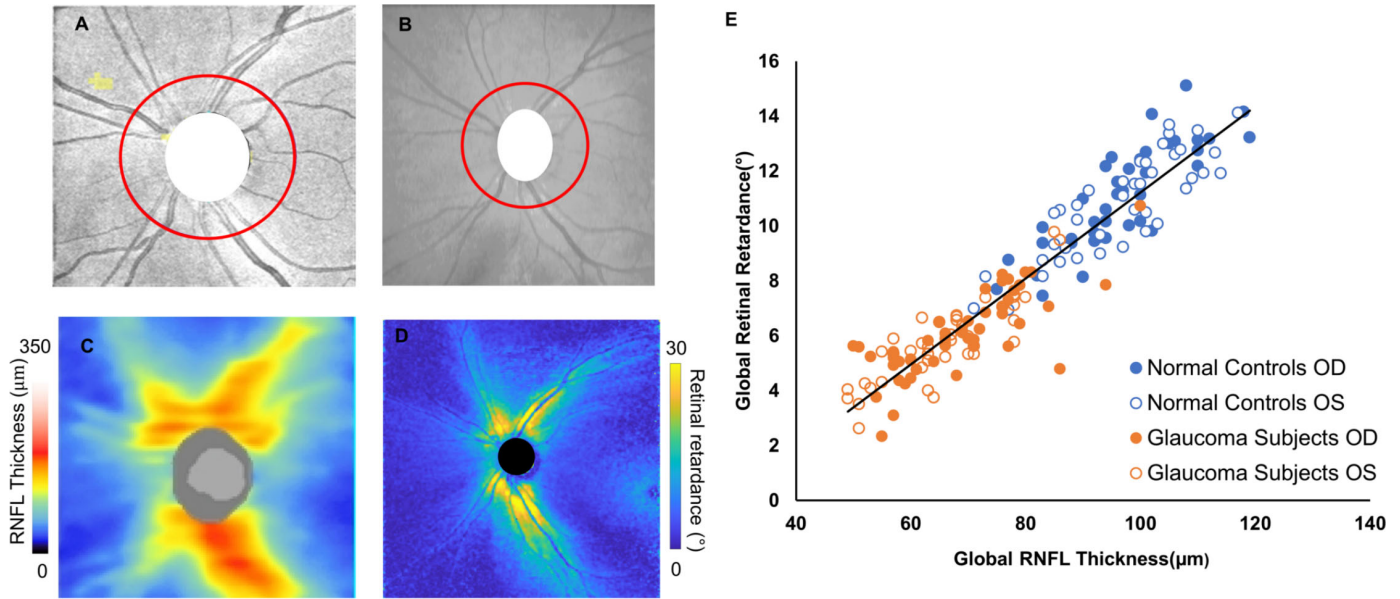|	Mean (SD)		
	Normal Controls ($n = 80$)	Glaucoma Participants ($n = 90$)	*P*
Global			
RR (°)	10.92 (1.85)	5.93 (1.51)	<0.001
RNFLT (µm)	96.68 (10.74)	67.4 (10.50)	<0.001
Superior quadrant			
RR (°)	16.71 (2.85)	8.27 (3.03)	<0.001
RNFLT (µm)	119.34 (24.72)	77.17 (16.07)	<0.001
Inferior quadrant			
RR (°)	16.12 (2.73)	7.27 (3.06)	<0.001
RNFLT (µm)	123.16 (18.09)	73.31 (19.32)	<0.001

Figure 5. RNFLT as measured by SD-OCT (ZEISS CIRRUS) versus RR as measured by PS-OCT. (**A**) Representative en face intensity map of a healthy eye measured by SD-OCT. (**B**) En face intensity map of the same eye measured by PS-OCT. (**C**) RNFLT map measured by SD-OCT. (**D**) En face retardance map measured by PS-OCT. (**E**) Correlation between average RNFLT measured by SD-OCT (ZEISS CIRRUS) and RR measured by PS-OCT ($n = 170$, $r = 0.94$, $P < 0.001$).

Table 4. Diagnostic Performance of Retinal Retardance and Thickness in Discrimination of Glaucoma

| Parameter	AUC (95% CI)	Sensitivity at ≥95% Specificity	P
Univariate analysis			
All glaucoma vs. normal controls			
Global RR (°)	0.98 (0.95–0.99)	93	0.553
Global RNFLT (µm)	0.97 (0.94–0.99)	93	
Early glaucoma vs. normal controls			
Global RR (°)	0.96 (0.91–0.98)	88	0.590
Global RNFLT (µm)	0.95 (0.89–0.98)	88	
Moderate glaucoma vs. normal controls			
Global RR (°)	0.99 (0.97–1.00)	96	0.454
Global RNFLT (µm)	0.98 (0.95–1.00)	81	
Severe glaucoma vs. normal controls			
Global RR (°)	1.00 (1.00–1.00)	100	0.999
Global RNFLT (µm)	1.00 (1.00–1.00)	100	
Multivariate analysis (adjusted for age, gender, and axial length)			
All glaucoma vs. normal controls			
Global RR (°)	0.99 (0.97–1.00)	93	0.737
Global RNFLT (µm)	0.99 (0.97–0.99)	92	
Early glaucoma vs. normal controls			
Global RR (°)	0.98 (0.95–0.99)	86	0.788
Global RNFLT (µm)	0.97 (0.94–0.99)	88	
Moderate glaucoma vs. normal controls			
Global RR (°)	1.00 (0.99–1.00)	100	0.479
Global RNFLT (µm)	0.99 (0.98–0.1.00)	93	
Severe glaucoma vs. normal controls			
Global RR (°)	1.00 (1.00–1.00)	100	0.999
Global RNFLT (µm)	1.00 (1.00–1.00)	100	
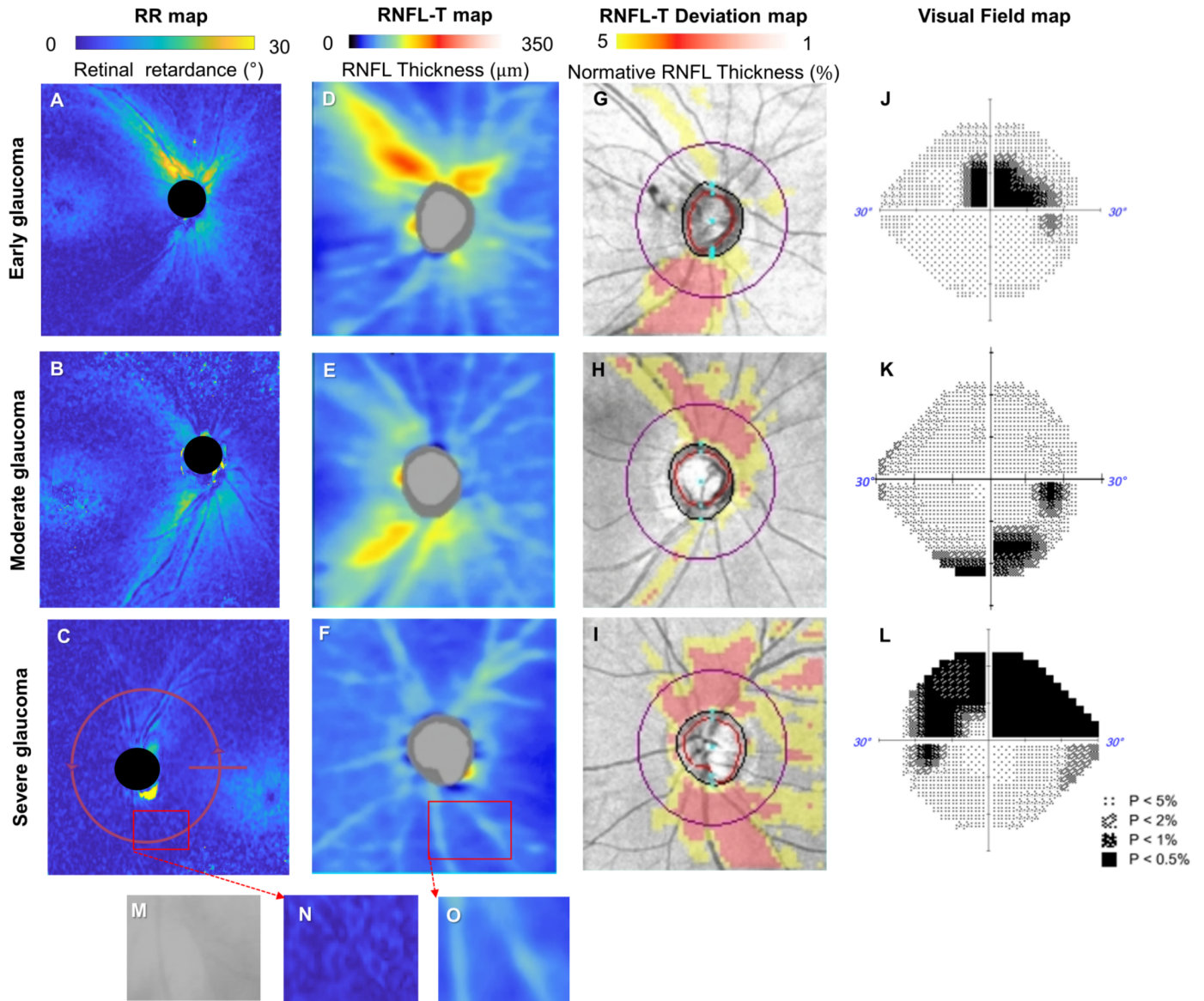
Figure 6. Comparison of VF-MD, RNFLT, and RR. (**A–C**) Representative examples of retardance en face maps from an early glaucoma eye with MD = −4.26 dB (**A**), moderate glaucoma eye with MD = −6.23 dB (**B**), and a severe glaucoma eye with MD = −14.80 dB (**C**). (**D–F**) RNFLT en face maps of the corresponding eyes. (**G–I**) RNFLT deviation maps. (**J–L**) Results from the VF central 24-2 threshold test. (**M–O**) PS-OCT intensity, PS-OCT retardance, and SD-OCT thickness maps focused on a small area indicted by *red boxes* (**C, F**) in a severe glaucomatous eye. The retinal vascular structures within the RNFL layer can be discerned from the thickness measurement. In contrast, in the RR map (**C, N**), the retinal vascular structures cannot be observed and do not contribute to the RR measurement. The *circular region* in (**C**) indicates the direction of the virtual B-scan.

glaucoma severity, in the context of results obtained from other existing diagnostic methods including SD-OCT and VF tests. In principle, the retardance measured by PS-OCT is closely related to the measurement made by scanning laser polarimetry,[17] also known as GDx, as both modalities measure the cumulative retardance of RNFL. The diagnostic performance of RR in this pilot study is consistent with previous reports of GDx, which have reported similar[32] but

slightly lower AUCs[33] than SD-OCT. Of note, in some early reports, the RNFL retardance as measured by GDx was regarded as the RNFLT under the assumption of a constant local birefringence; however, this assumption was proved invalid by PS-OCT, as the local birefringence in RNFL was significantly lower in eyes with glaucoma than in healthy ones.[15,20] Compared to GDx, PS-OCT provides three-dimensional imaging of the retina and excludes the light backscat-
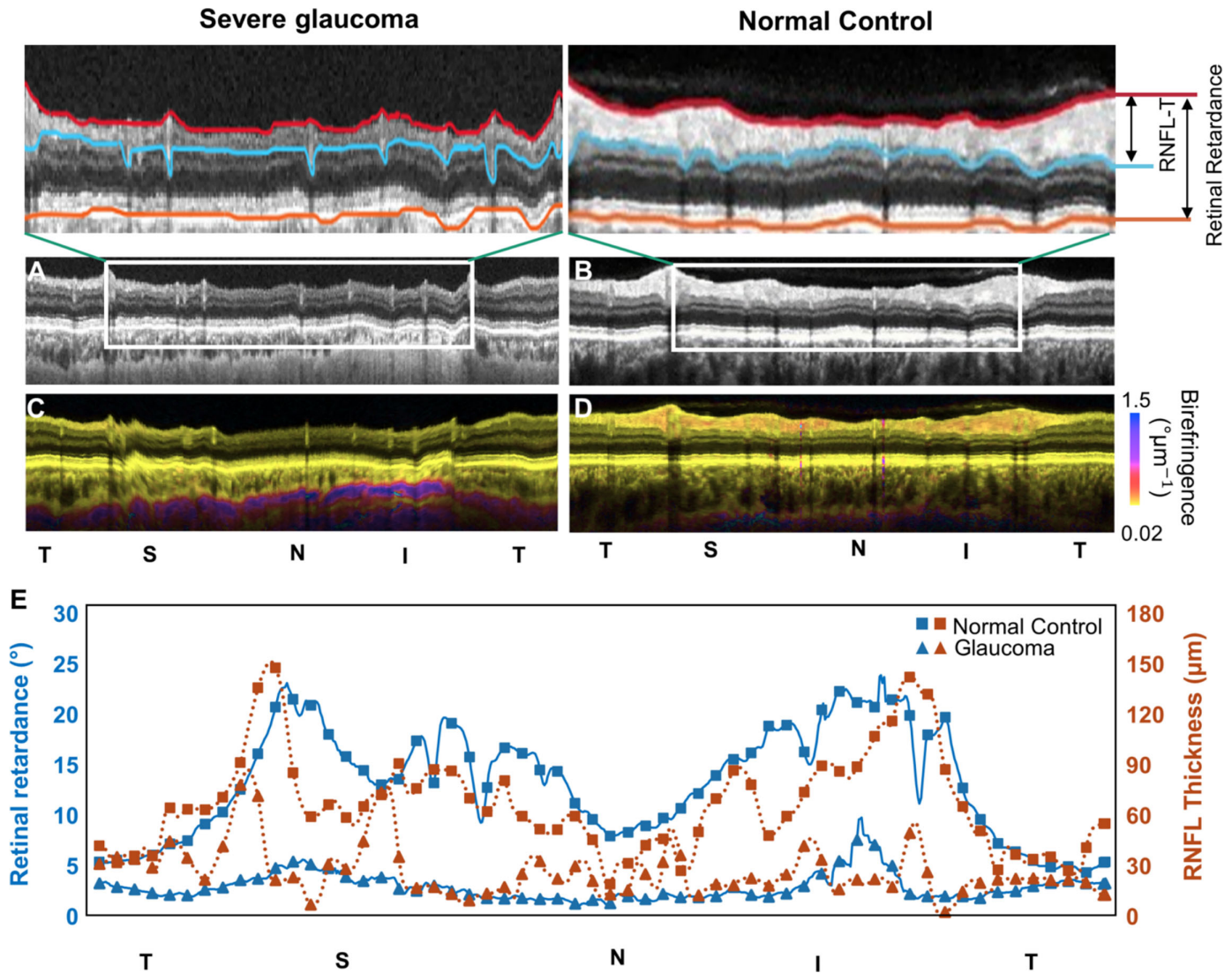
Figure 7. (**A**, **B**) Virtual circular B-scans of an eye with severe glaucoma (**A**) and a normal control eye (**B**) extracted around the optic nerve head at 3.5-mm diameter starting at the superotemporal region. A closer look at the superior, nasal, and inferior regions of the retina reveals that, in severe glaucoma, along with the apparent thinning of the RNFL layer compared to normal controls the retinal blood vessels extend beyond the RNFL floor, compromising the reliability of the segmentation of the RNFL floor. The *red* and *orange lines* indicate the boundaries of segmentation for RR measurement, and the *red* and *blue lines* indicate the bounds of segmentation for RNFLT measurement. (**C**, **D**) Distribution of retardance in the retinal layers of an eye with severe glaucoma and normal control, respectively. (**E**) RR–RNFLT plot. This plot reveals peaks in the thickness measurement of the severe glaucoma eye influenced by the blood vessels.

tered from the choroid and sclera, thus providing more reliable information on the RNFL properties than the two-dimensional measurement made by GDx.[34]

It has been speculated that PS-OCT may help diagnose early glaucoma under the assumption that a loss of birefringence may occur before the change of thickness in RNFL.[12,15] Our current results do not support this speculation because we observed that the RNFLT and RR exhibited similar diagnostic performance in eyes with early glaucoma. This

finding still requires further investigation, as we used VF-MD to classify early glaucoma in this pilot study. VF testing may not be sensitive to early glaucoma, as the vision may not be affected until more than 20% to 40% of ganglion cells have been damaged.[26,35] The birefringence properties of RNFL in an earlier stage of glaucoma before detectable VF loss was not assessed in this pilot study. In addition, in this pilot study only the total retardance projected from the retinal surface to RPE was assessed for its diagnostic performance and structure–function correlation,

Table 5. Spearman's Correlation Coefficient (r) for Correlation Among Global RR, RNFLT, and VF-MD Within the Various Glaucoma Groups

	All Glaucoma			Early Glaucoma (n = 43 Eyes, 34 Subjects)			Moderate Glaucoma (n = 27 Eyes, 26 Subjects)			Severe Glaucoma (n = 20 Eyes, 20 Subjects)		
	r	P	Z	r	P	Z	r	P	Z	r	P	Z
Univariate analysis												
RR (°) – VF-MD	0.68	**<0.001**	**1.99** (**P = 0.047**)	0.22	0.146	0.78 (P = 0.437)	0.55	**0.003**	−0.83 (P = 0.407)	0.73	**<0.001**	**1.96** (**P = 0.050**)
RNFLT (µm) – VF-MD	0.58	**<0.001**		0.14	0.360		0.66	**<0.001**		0.43	0.061	
RR – RNFLT	0.80	**<0.001**		0.79	**<0.001**		0.62	**<0.001**		0.63	**0.003**	
Multivariate analysis (adjusted for age, gender, and axial length)												
RR (°) – VF-MD	0.67	**<0.001**	**1.96** (**P = 0.050**)	0.19	0.233	0.76 (P = 0.449)	0.56	**0.004**	−0.93 (P = 0.355)	0.72	**0.001**	**2.08** (**P = 0.038**)
RNFLT (µm) – VF-MD	0.57	**<0.001**		0.11	0.49		0.68	**<0.001**		0.42	0.095	
RR – RNFLT	0.80	**<0.001**		0.77	**<0.001**		0.62	**0.001**		0.68	**0.003**	

Boldface values indicate statistical significance at $P < 0.05$.

as the depth-resolved birefringence of RNFL did not serve as an effective indicator in moderate and severe glaucoma cases in comparison with retinal retardance.

The pilot study has certain limitations that should be considered when interpreting the results. First, it has been reported that age-related RNFL loss can be difficult to differentiate from glaucomatous RNFL thinning.[36] Therefore, the AUCs of the diagnostic metrics reported in our study are likely to be affected by age, given that the glaucoma subjects were significantly older than the normal controls.[36] To mitigate this issue, we adjusted for the potential confounding effect of age by including it as an independent variable in the analysis, thus ensuring that our observed effects were not solely due to the influence of aging. Second, the limited sample size has led to relatively large uncertainty in the diagnostic performance analysis of this pilot study and highlights the needs for future studies with larger cohorts to validate our initial observations. Validating PS-OCT to monitor glaucoma progression requires more evidence from a longitudinal study on a severe glaucoma population. Third, a relatively large portion of data (19%, due to low-quality scans from PS-OCT and SD-OCT) was excluded due to positioning issues and motion artifacts because the PS-OCT prototype used in this pilot study lacked standard alignment-aiding techniques, including fundus preview, automatic depth positioning unit, and retina motion tracker. Also, the comparison of RR and RNFLT was based on measurements from two different devices, which may introduce measurement variations due to differences in scanning areas, sampling parameters, surface detection algorithms, laser wavelengths, and optics used for imaging. Future studies will consider these factors and match the imaging parameters between devices under comparison.

Finally, we utilized single-visit VF tests in our analysis, supported by reliable scans with a low percentage of fixation losses and false negatives (<15%). Yet, it is acknowledged that this approach may introduce variability, particularly in cases of moderate to severe glaucoma.[11] Future investigations incorporating larger cohorts and follow-up visits are recommended to ensure more robust and conclusive outcomes. Moreover, the observed nonlinear relationship between retinal retardance and VF-MD prompts further exploration into the implications of birefringent properties and their spatial dependency.

In conclusion, PS-OCT shows promising results as a potential tool for monitoring the progression of glaucoma, warranting further large-scale, longitudinal studies.
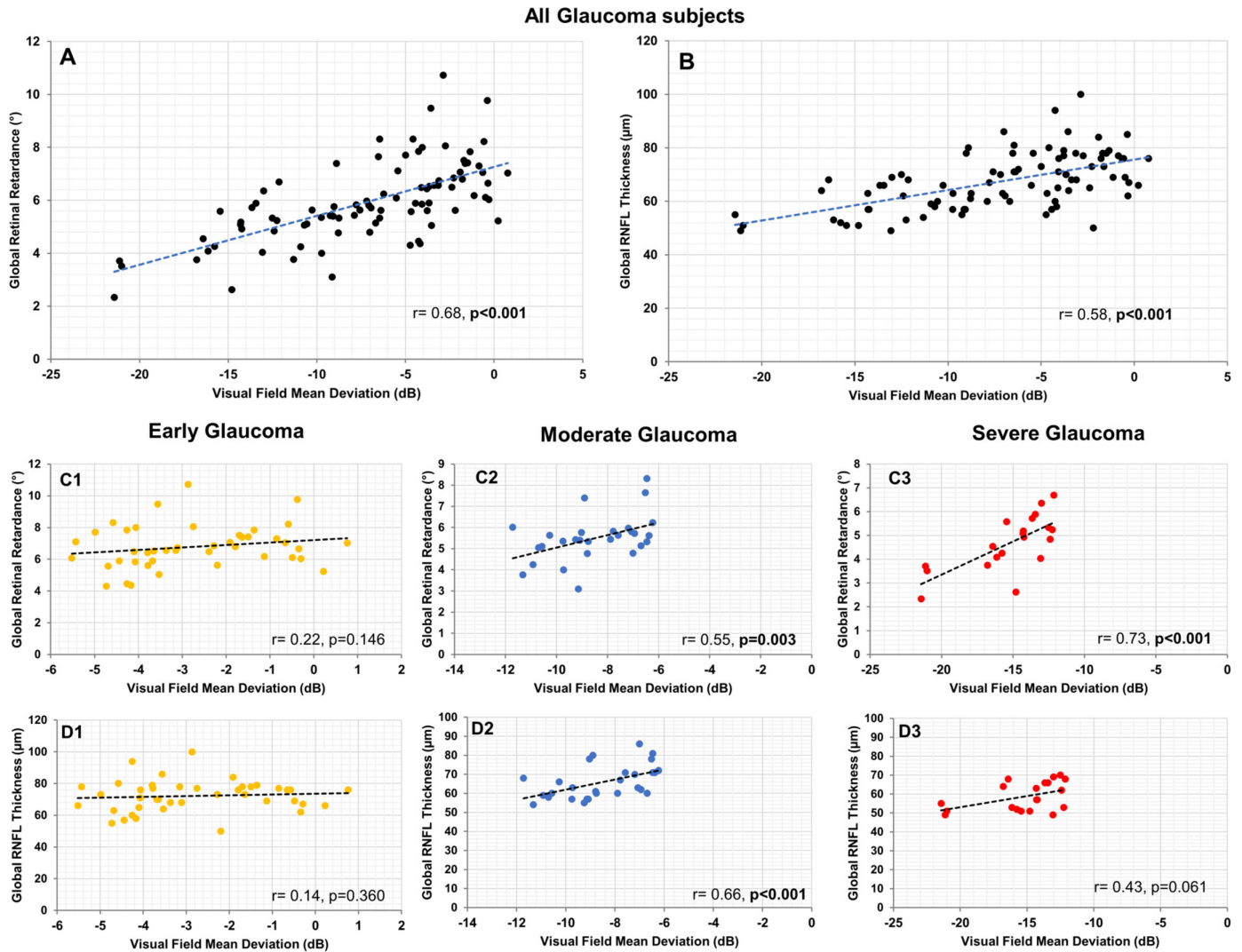
Figure 8. Correlation analysis of RR, RNFLT, and VF-MD in all glaucoma subjects and groups of early, moderate, and severe glaucoma. (**A**) Correlation between VF-MD and RR in all glaucoma subjects ($r = 0.68$, $P < 0.001$). (**B**) Correlation between VF-MD and RNFLT in all glaucoma subjects ($r = 0.58$, $P < 0.001$). (**C1–C3**) Correlation between VF-MD and RR in early ($r = 0.22$, $P = 0.146$), moderate ($r = 0.55$, $P = 0.003$), and severe glaucoma ($r = 0.73$, $P < 0.001$) groups. (**D1–D3**) Correlation between VF-MD and RNFLT in early ($r = 0.14$, $P = 0.360$), moderate ($r = 0.66$, $P < 0.001$), and severe glaucoma ($r = 0.43$, $P = 0.061$) groups. The *dashed lines* on the plots represent the lines of best fit.

References

1. Bussel II, Wollstein G, Schuman JS. OCT for glaucoma diagnosis, screening and detection

of glaucoma progression. *Br J Ophthalmol*. 2014;98(suppl. 2):ii15–ii19.

2. Leung CK, Cheung CY, Weinreb RN, et al. Retinal nerve fiber layer imaging with spectral-domain optical coherence tomography: a variability and diagnostic performance study. *Ophthalmology*. 2009;116(7):1257–1263.e2.

3. Broadway DC. Visual field testing for glaucoma – a practical guide. *Community Eye Health*. 2012;25(79–80):66–70.

4. Artes PH, Nicolela MT, LeBlanc RP, Chauhan BC. Visual field progression in glaucoma: total versus pattern deviation analyses. *Invest Ophthalmol Vis Sci*. 2005;46(12):4600–4606.

5. Ye C, Yu M, Leung CK. Impact of segmentation errors and retinal blood vessels on retinal nerve fibre layer measurements using spectral-domain optical coherence tomography. *Acta Ophthalmol*. 2016;94(3):e211–e219.

6. Nagarkatti-Gude N, Gardiner SK, Fortune B, Demirel S, Mansberger SL. Optical coherence tomography segmentation errors of the retinal nerve fiber layer persist over time. *J Glaucoma*. 2019;28(5):368–374.

7. Mansberger SL, Menda SA, Fortune BA, Gardiner SK, Demirel S. Automated segmentation errors when using optical coherence tomography to measure retinal nerve fiber layer thickness in glaucoma. *Am J Ophthalmol*. 2017;174:1–8.

8. Bowd C, Zangwill LM, Weinreb RN, Medeiros FA, Belghith A. Estimating optical coherence tomography structural measurement floors to improve detection of progression in advanced glaucoma. *Am J Ophthalmol*. 2017;175:37–44.

9. Iikawa R, Togano T, Sakaue Y, et al. Estimation of the central 10-degree visual field using en-face images obtained by optical coherence tomography. *PLoS One*. 2020;15(3):e0229867.

10. Shuldiner SR, Boland MV, Ramulu PY, et al. Predicting eyes at risk for rapid glaucoma progression based on an initial visual field test using machine learning. *PLoS One*. 2021;16(4):e0249856.

11. Gardiner SK, Swanson WH, Goren D, Mansberger SL, Demirel S. Assessment of the reliability of standard automated perimetry in regions of glaucomatous damage. *Ophthalmology* 2014;121(7):1359–1369.

12. Pircher M, Hitzenberger CK, Schmidt-Erfurth U. Polarization sensitive optical coherence tomography in the human eye. *Prog Retin Eye Res*. 2011;30(6):431–451.

13. Braaf B, Vermeer KA, de Groot M, Vienola KV, de Boer JF. Fiber-based polarization-sensitive OCT of the human retina with correction of system polarization distortions. *Biomed Opt Express*. 2014;5(8):2736–2758.

14. Desissaire S, Pollreisz A, Sedova A, et al. Analysis of retinal nerve fiber layer birefringence in patients with glaucoma and diabetic retinopathy by polarization sensitive OCT. *Biomed Opt Express*. 2020;11(10):5488–5505.

15. Steiner S, Schwarzhans F, Desissaire S, et al. Birefringent properties of the peripapillary retinal nerve fiber layer in healthy and glaucoma subjects analyzed by polarization-sensitive OCT. *Invest Ophthalmol Vis Sci*. 2022;63(12):8.

16. Cense B, Chen TC, Park BH, Pierce MC, de Boer JF. Thickness and birefringence of healthy retinal nerve fiber layer tissue measured with polarization-sensitive optical coherence tomography. *Invest Ophthalmol Vis Sci*. 2004;45(8):2606–2612.

17. Yamanari M, Miura M, Makita S, Yatagai T, Yasuno Y. Phase retardation measurement of retinal nerve fiber layer by polarization-sensitive spectral-domain optical coherence tomography and scanning laser polarimetry. *J Biomed Opt*. 2008;13(1):014013.

18. Elmaanaoui B, Wang B, Dwelle JC, et al. Birefringence measurement of the retinal nerve fiber layer by swept source polarization sensitive optical coherence tomography. *Opt Express*. 2011;19(11):10252–10268.

19. Götzinger E, Pircher M, Baumann B, Hirn C, Vass C, Hitzenberger CK. Retinal nerve fiber layer birefringence evaluated with polarization sensitive spectral domain OCT and scanning laser polarimetry: a comparison. *J Biophotonics*. 2008;1(2):129–139.

20. Zotter S, Pircher M, Götzinger E, et al. Measuring retinal nerve fiber layer birefringence, retardation, and thickness using wide-field, high-speed polarization sensitive spectral domain OCT. *Invest Ophthalmol Vis Sci*. 2013;54(1):72–84.

21. Liu X, Jiang L, Ke M, et al. Posterior scleral birefringence measured by triple-input polarization-sensitive imaging as a biomarker of myopia progression. *Nat Biomed Eng*. 2023;7(8):986–1000.

22. Mills RP, Budenz DL, Lee PP, et al. Categorizing the stage of glaucoma from pre-diagnosis to end-stage disease. *Am J Ophthalmol*. 2006;141(1):24–30.

23. Carl Zeiss Meditec. *CIRRUS HD-OCT User Manual*. Jena, Germany: Carl Zeiss Meditec; 2020.

24. Li Q, Karnowski K, Untracht G, et al. Vectorial birefringence imaging by optical coherence microscopy for assessing fibrillar microstructures

in the cornea and limbus. *Biomed Opt Express*. 2020;11(2):1122–1138.

25. Bengtsson B, Heijl A. SITA Fast, a new rapid perimetric threshold test. Description of methods and evaluation in patients with manifest and suspect glaucoma. *Acta Ophthalmol Scand*. 1998;76(4):431–437.

26. El-Naby AA, Abouelkheir H, Al-Sharkawy H, Mokbel T. Correlation of retinal nerve fiber layer thickness and perimetric changes in primary open-angle glaucoma. *J Egypt Ophthalmol Soc*. 2018;111(1):7–14.

27. Tan B, Lim NA, Tan R, et al. Combining retinal and choroidal microvascular metrics improves discriminative power for diabetic retinopathy. *Br J Ophthalmol*. 2023;107(7):993–999.

28. Ratcliffe SJ, Shults J. GEEQBOX: a MATLAB toolbox for generalized estimating equations and quasi-least squares. *J Stat Softw*. 2008;25(14):1–14.

29. DeLong ER, DeLong DM, Clarke-Pearson DL. Comparing the areas under two or more correlated receiver operating characteristic curves: a nonparametric approach. *Biometrics*. 1988;44(3):837–845.

30. Steiger JH. Tests for comparing elements of a correlation matrix. *Psychol Bull*. 1980;87(2):245–251.

31. Yow AP, Chua J, Tan B, et al. Neurovascular segregation of the retinal nerve fiber layer in glaucoma. *Ann N Y Acad Sci*. 2023;1528(1):95–103.

32. Medeiros FA, Zangwill LM, Bowd C, Weinreb RN. Comparison of the GDx VCC scanning laser polarimeter, HRT II confocal scanning laser ophthalmoscope, and stratus OCT optical coherence tomograph for the detection of glaucoma. *Arch Ophthalmol*. 2004;122(6):827–837.

33. Rao HL, Yadav RK, Addepalli UK, et al. Peripapillary retinal nerve fiber layer assessment of spectral domain optical coherence tomography and scanning laser polarimetry to diagnose preperimetric glaucoma. *PLoS One*. 2014;9(10):e108992.

34. Götzinger E, Pircher M, Baumann B, Hirn C, Vass C, Hitzenberger CK. Analysis of the origin of atypical scanning laser polarimetry patterns by polarization-sensitive optical coherence tomography. *Invest Ophthalmol Vis Sci*. 2008;49(12):5366–5372.

35. Morgan JE, Uchida H, Caprioli J. Retinal ganglion cell death in experimental glaucoma. *Br J Ophthalmol*. 2000;84(3):303–310.

36. Wong D, Chua J, Baskaran M, et al. Factors affecting the diagnostic performance of circumpapillary retinal nerve fibre layer measurement in glaucoma. *Br J Ophthalmol*. 2021;105(3):397–402.

translational vision science & technology